50-kHz-rate 2D imaging of temperature and H_2O concentration at the exhaust plane of a J85 engine using hyperspectral tomography

Lin Ma,[1,*] Xuesong Li,[1] Scott T. Sanders,[2] Andrew W. Caswell,[3]
Sukesh Roy,[3] David H. Plemmons,[4] and James R. Gord[5]

[1]*Department of Aerospace and Ocean Engineering, Virginia Tech, Blacksburg, Virginia 24060, USA*
[2]*Department of Mechanical Engineering, University of Wisconsin-Madison, Madison, Wisconsin 53706, USA*
[3]*Spectral Energies LLC, 5100 Springfield Street, Suite 301, Dayton, Ohio 45431, USA*
[4]*Aerospace Testing Alliance, Arnold AFB, Tennessee 37389, USA*
[5]*Air Force Research Laboratory, Propulsion Directorate, Wright-Patterson AFB, Ohio 45433, USA*
[*]*LinMa@vt.edu*

Abstract: This paper describes a novel laser diagnostic and its demonstration in a practical aero-propulsion engine (General Electric J85). The diagnostic technique, named hyperspectral tomography (HT), enables simultaneous 2-dimensional (2D) imaging of temperature and water-vapor concentration at 225 spatial grid points with a temporal response up to 50 kHz. To our knowledge, this is the first time that such sensing capabilities have been reported. This paper introduces the principles of the HT techniques, reports its operation and application in a J85 engine, and discusses its perspective for the study of high-speed reactive flows.

©2013 Optical Society of America

OCIS codes: (100.6950) Tomographic image processing; (280.1740) Combustion diagnostics.

References and links

1. R. K. Hanson, "Applications of quantitative laser sensors to kinetics, propulsion and practical energy systems," Proc. Combust. Inst. **33**(1), 1–40 (2011).
2. K. Kohse-Hoinghaus, R. S. Barlow, M. Alden, and E. Wolfrum, "Combustion at the focus: laser diagnostics and control," Proc. Combust. Inst. **30**(1), 89–123 (2005).
3. F. Mayinger and O. Feldmann, *Optical Measurements: Techniques and Applications* (Springer, 2001).
4. A. C. Eckbreth, *Laser Diagnostics for Combustion Temperature and Species* (Gordon and Breach Publishers, 1996).
5. R. S. Barlow, "Laser diagnostics and their interplay with computations to understand turbulent combustion," Proc. Combust. Inst. **31**(1), 49–75 (2007).
6. I. Boxx, M. Stohr, C. Carter, and W. Meier, "Sustained multi-kHz flamefront and 3-component velocity-field measurements for the study of turbulent flames," Appl. Phys. B **95**(1), 23–29 (2009).
7. M. Stoehr, I. Boxx, C. Carter, and W. Meier, "Dynamics of lean blowout of a swirl-stabilized flame in a gas turbine model combustor," Proc. Combust. Inst. **33**(2), 2953–2960 (2011).
8. B. H. Cheung and R. K. Hanson, "CW laser-induced fluorescence of toluene for time-resolved imaging of gaseous flows," Appl. Phys. B **98**(2-3), 581–591 (2010).
9. K. N. Gabet, R. A. Patton, N. Jiang, W. R. Lempert, and J. A. Sutton, "High-speed CH_2O PLIF imaging in turbulent flames using a pulse-burst laser system," Appl. Phys. B **106**(3), 569–575 (2012).
10. N. Jiang, M. Webster, W. R. Lempert, J. D. Miller, T. R. Meyer, C. B. Ivey, and P. M. Danehy, "MHz-rate nitric oxide planar laser-induced fluorescence imaging in a Mach 10 hypersonic wind tunnel," Appl. Opt. **50**(4), A20–A28 (2011).
11. D. Hoffman, K. U. Münch, and A. Leipertz, "Two-dimensional temperature determination in sooting flames by filtered Rayleigh scattering," Opt. Lett. **21**(7), 525–527 (1996).
12. P. J. Emmerman, R. Goulard, R. J. Santoro, and H. G. Semerjian, "Multi-angular absorption diagnostics of a turbulent argon-methane jet," J. Energy **4**(2), 70–77 (1980).
13. P. Paci, Y. Zvinevich, S. Tanimura, B. E. Wyslouzil, M. Zahniser, J. Shorter, D. Nelson, and B. McManus, "Spatially resolved gas phase composition measurements in supersonic flows using tunable diode laser absorption spectroscopy," J. Chem. Phys. **121**(20), 9964–9970 (2004).
14. A. M. Chojnacki, G. J. Wolga, and F. C. Gauldin, "Infrared color center laser system for tomographic determination of temperature and species concentration distributions in combusting systems," Combust. Sci. Technol. **134**(1-6), 165–181 (1998).
15. R. Villarreal and P. L. Varghese, "Frequency-resolved absorption tomography with tunable diode lasers," Appl. Opt. **44**(31), 6786–6795 (2005).

16. P. Wright, C. A. Garcia-Stewart, S. J. Carey, F. P. Hindle, S. H. Pegrum, S. M. Colbourne, P. J. Turner, W. J. Hurr, T. J. Litt, S. C. Murray, S. D. Crossley, K. B. Ozanyan, and H. McCann, "Toward in-cylinder absorption tomography in a production engine," Appl. Opt. **44**(31), 6578–6592 (2005).
17. C. T. Herman, "Image reconstruction from projections - the fundamentals of computerized tomography," in *Computer Science and Applied Mathematics* (Academic Press, 1980).
18. W. Cai, D. J. Ewing, and L. Ma, "Application of simulated annealing for multispectral tomography," Comput. Phys. Commun. **179**(4), 250–255 (2008).
19. L. Ma and W. Cai, "Determination of the optimal regularization parameters in hyperspectral tomography," Appl. Opt. **47**(23), 4186–4192 (2008).
20. L. Ma and W. Cai, "Numerical investigation of hyperspectral tomography for simultaneous temperature and concentration imaging," Appl. Opt. **47**(21), 3751–3759 (2008).
21. L. Ma, W. Cai, A. W. Caswell, T. Kraetschmer, S. T. Sanders, S. Roy, and J. R. Gord, "Tomographic imaging of temperature and chemical species based on hyperspectral absorption spectroscopy," Opt. Express **17**(10), 8602–8613 (2009).
22. X. An, T. Kraetschmer, K. Takami, S. T. Sanders, L. Ma, W. Cai, X. Li, S. Roy, and J. R. Gord, "Validation of temperature imaging by H_2O absorption spectroscopy using hyperspectral tomography in controlled experiments," Appl. Opt. **50**(4), A29–A37 (2011).
23. K. P. Savage, G. R. Beitel, R. S. Hiers, and R. J. Schulz, "Test capabilities in the AEDC/UTSI J85 turbojet test stand," in *2007 U. S. Air Force T&E Days* (*AIAA*, 2007)
24. L. A. Kranendonk, X. An, A. W. Caswell, R. E. Herold, S. T. Sanders, R. Huber, J. G. Fujimoto, Y. Okura, and Y. Urata, "High speed engine gas thermometry by Fourier-domain mode-locked laser absorption spectroscopy," Opt. Express **15**(23), 15115–15128 (2007).
25. S. I. Chou, D. S. Baer, R. K. Hanson, W. Z. Collison, and T. Q. Ni, "HBr concentration and temperature measurements in a plasma etch reactor using diode laser absorption spectroscopy," J. Vac. Sci. Technol. A **19**(2), 477–484 (2001).
26. T. Kraetschmer, D. Dagel, and S. T. Sanders, "Simple multiwavelength time-division multiplexed light source for sensing applications," Opt. Lett. **33**(7), 738–740 (2008).
27. A. W. Caswell, T. Kraetschmer, K. Rein, S. T. Sanders, S. Roy, D. T. Shouse, and J. R. Gord, "Application of time-division-multiplexed lasers for measurements of gas temperature and CH_4 and H_2O concentrations at 30 kHz in a high-pressure combustor," Appl. Opt. **49**(26), 4963–4972 (2010).
28. C. Jirauschek, B. Biedermann, and R. Huber, "A theoretical description of Fourier domain mode locked lasers," Opt. Express **17**(26), 24013–24019 (2009).
29. X. An, A. W. Caswell, J. J. Lipor, and S. T. Sanders, "Determining the optimum wavelength pairs to use for molecular absorption thermometry based on the continuous-spectral lower-state energy," J. Quant. Spectrosc. Radiat. Transf. **112**(14), 2355–2362 (2011).
30. L. Ma, X. Li, W. Cai, S. Roy, J. R. Gord, and S. T. Sanders, "Selection of multiple optimal absorption transitions for nonuniform temperature sensing," Appl. Spectrosc. **64**(11), 1274–1282 (2010).

1. Introduction

The study of reactive flows continues to challenge diagnosticians with the need for non-intrusive techniques that can provide quantitative measurements with adequate temporal and spatial resolution [1]. Such measurements have been repeatedly shown to be invaluable for the validation of existing models and also for the inspiration of new models. These techniques are furthermore desired to be robust and suitable for *in situ* monitoring and control purposes in practical combustion and propulsion systems to improve their efficiency and performance [2].

Among the properties important for reactive flows, temperature and concentration of chemical species are two most important ones; and the corresponding developments of diagnostic techniques have attracted a tremendous amount of research efforts. This paper reports a new laser diagnostic that can measure 2-dimensional (2D) distribution of temperature and concentration of water vapor (H_2O) simultaneously with a temporal resolution of 50 kHz and a spatial resolution of 225 (15 × 15) grid points. The HT technique utilizes multiple line-of-sight-averaged measurements of the absorption spectra of H_2O vapor to infer the distribution of temperature and H_2O concentration. To our knowledge, this is the first time that such measurement capabilities have been reported. The technique has been demonstrated in the exhaust plane of a practical aero-propulsion engine (General Electric J85).

Here we have to limit the review of related work to recent efforts that aim at high-speed and 2D imaging of temperature and chemical species for two reasons. First, a complete survey, even a brief one, will be beyond the scope of this current paper because of the volume of past literature. Second, there already exist excellent monographs [3, 4] and dedicated

reviews [1, 5] that provide a thorough discussion of past research in the non-intrusive measurement of temperature and chemical species.

For 2D measurement of the concentration of chemical species, the well-established technique is planar laser-induced fluorescence (PLIF) [4]. The temporal resolution of PLIF is largely driven by the availability of high-speed lasers, cameras, and intensifiers. With such hardware becoming commercially available recently, multi-kHz PLIF systems have gradually become at more and more researchers' disposal [6–8]. Customer-built laser systems can further extend PLIF measurements to tens of kHz [9, 10], comparable to that of the HT technique reported here. The spatial resolution of PLIF is typically well below a millimeter, significantly superior to the HT technique demonstrated in this current work (38.3 mm, or 1.5 inches). Note however that 1) the spatial resolution of the HT technique is fundamentally limited by the size of the laser beam and can be dramatically improved beyond 38.3 mm, and 2) our current implementation of the HT technique essentially trades spatial resolution for the field-of-view (FOV). The current HT implementation monitored a 57×57 cm (22.5×22.5 inches) region. The spatial resolution can be improved by decreasing the size of the FOV, a trade-off that PLIF faces too.

For 2D measurement of temperature, Rayleigh scattering represents a well-established technique [4]. The comparison between Rayleigh scattering and the HT technique is similar to that between PLIF and HT. The temporal resolution of Rayleigh scattering is again largely driven by the availability of hardware, and can reach comparable level as reported here. The spatial resolution of typical Rayleigh scattering is superior to that of the HT technique reported here, and trade-off between spatial resolution and the size of the FOV applies to Rayleigh scattering too.

Comparison of HT to PLIF and Rayleigh scattering in other aspects (besides temporal and spatial resolution and the FOV) provides further motivation for the HT technique. For example, quantitative interpretation of PLIF measurements requires independent information of temperature and local quenching rates, which can be difficult or even impossible to obtain in practical reactive flows. The Rayleigh signal depends on local gas composition, which can make the signal indecipherable in reactive flows. Furthermore, Rayleigh signal is relatively weak because of its non-resonant and elastic nature. As a result, conventional Rayleigh scattering is susceptible to interference due to particulate/droplet scattering and surface reflection, restricting its practical applications, and laser diagnosticians have been investigating techniques such as filtered Rayleigh scattering [11] to overcome these issues. Lastly, the laser equipments involved in PLIF and Rayleigh scattering are typically not fiber coupled, requiring their implementation to be in close proximity to the target test rig. Such requirements often pose significant challenges in practice because of the harsh environment created by combustion and propulsion systems, and these challenges are further compounded by the relatively bulky size of the laser equipment involved with PLIF and Rayleigh techniques.

The HT technique described in this work addresses these practical issues mentioned above. The HT technique provides simultaneous temperature and H_2O concentration measurements, with no requirement of other additional measurements or calibrations. The technique is fully fiber coupled, portable, and robust for practical applications. These advantages will become evident when the experimental arrangement is described in Section 3. In the next section, we briefly introduce the background of absorption tomography and the mathematical formulation of the HT technique.

2. Background of hyperspectral tomography

The HT technique combines the use of tomography with hyperspectral absorption spectroscopy to extend the capabilities of traditional absorption-based diagnostics. Compared with previous work on absorption-based tomography, the HT technique exploits the spectral information at a large number of absorption transitions whereas previous work relied on spectral information at a limited number of transitions (typically one or two) [12–16]. Hence, the HT technique essentially adds wavelength as a new dimension to the traditional

tomography problem, which primarily focused on the use of spatial information [17]. Our study thus far [18–22] has suggested that the increased spectral information content offer several important advantages including the reduction of the number of projections required for a faithful tomographic reconstruction, improved resistance to measurement noise, and the ability to obtain simultaneous temperature and concentration imaging.

The concept, mathematical formulation, numerical evaluation, demonstration, and validation of the HT technique have been detailed in a series of previous work. The concept and mathematical formulation were introduced in [18, 20], the numerical evaluation was described in [19, 20], a prototype HT sensor was demonstrated in a laboratory flame in [21], and the validation of the full-scale sensor used in this work was reported in [22]. With these previously documented efforts, this section intends only to provide a brief summary of the physics and mathematics of HT to facilitate the discussion in the rest of the paper.

Figure 1 depicts the HT problem. A hyperspectral laser beam is directed along the line of sight, denoted by l, to probe the domain of interest as shown in the left panel. Absorption by the target species will attenuate the probe laser beam, and the absorbance at a certain wavelength (e.g., λ_i) generally contains contributions from multiple transitions centered at various wavelengths (including that centered at λ_i itself), as schematically shown in the right panel. Here, we use $p(L_j, \lambda_i)$, termed a projection, to denote the absorbance at a projection location L_j and a wavelength λ_i. The projection, $p(L_j, \lambda_i)$, is expressed by the following integral:

$$p\left(L_j, \lambda_i\right) = \int_a^b \sum_k S\left(\lambda_k, T\left(\ell\right)\right) \cdot X\left(\ell\right) \cdot \Phi\left(\lambda_k - \lambda_i\right) \cdot P \cdot d\ell \qquad (1)$$

where a and b are the integration limits determined by the line of sight and the geometry of the domain of interest, $S(\lambda_k, T(l))$ is the line strength of the contributing transition centered at a wavelength λ_k and depends nonlinearly on temperature (T); $T(l)$ and $X(l)$ are the temperature and mole-fraction profile of the absorbing species along the line of sight, respectively; Φ is the Voigt lineshape function; and P is the pressure, assumed to be uniform. The summation runs over all the transitions with non-negligible contributions. In this work, the domain of interest is discretized by superimposing a square mesh in the Cartesian coordinate, as shown in the left panel of Fig. 1; and the integration in Eq. (1) is also discretized accordingly.
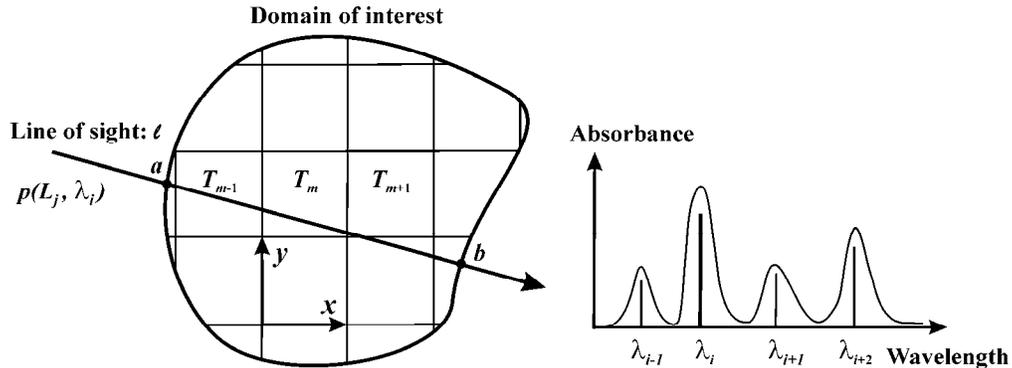

Fig. 1. The mathematical formulation of the hyperspectral tomography problem.

The HT problem seeks to determine the distributions of T and X over the discretized domain with a finite set of projections as described in Eq. (1). We developed a method to cast the inversion problem into a nonlinear optimization problem, where the T and X distributions are retrieved by minimizing the following function:

$$D(T^{rec}, X^{rec}) = \sum_{j=1}^{J} \sum_{i=1}^{I} \frac{[p_m(L_j, \lambda_i) - p_c(L_j, \lambda_i)]^2}{p_m(L_j, \lambda_i)^2} \qquad (2)$$

where $p_m(L_j, \lambda_i)$ denotes the measured projection at a location L_j and a wavelength λ_i; $p_c(L_j, \lambda_i)$ the computed projection based on a reconstructed T and X profile (denoted by T^{rec} and X^{rec}, respectively); and J and I the total number of wavelengths and projection locations used in the tomography scheme, respectively. This function, D, provides a quantitative measure of the closeness between the reconstructed and the actual temperature and concentration profiles. The contribution from each wavelength to D is normalized by the projection at this wavelength itself, such that projections measured at all wavelengths are weighted equally in the inversion. In an ideal case where the measurements are noise free, D reaches its global minimum (zero) when T^{rec} and X^{rec} match the actual profiles.

The formulation in Eq. (2) allows the flexible incorporation of available *a priori* information via regulation. For instance, in practice, the T and X distribution sought are non-negative, bounded, and smooth to a certain degree because of thermal and mass diffusion. All such information is included in minimizing Eq. (2) [19, 20]. More specifically, the non-negativity and boundedness regularizations are incorporated in the minimization algorithm (the simulated annealing algorithm), and the smoothness regularization is implemented by modifying the target function D into:

$$F(T^{rec}, X^{rec}) = D(T^{rec}, X^{rec}) + \gamma_T \cdot R_T(T^{rec}) + \gamma_X \cdot R_X(X^{rec}) \qquad (3)$$

where R_T and R_X are the regularization factors for temperature and concentration, respectively; γ_T and γ_X are positive constants (regularization parameters) to scale the magnitude of R_T and R_X properly. More details of the use of regularization factors, the determination of the optimal regularization parameters, and the simulated annealing algorithm can be found in [18–20]. Finally, the solution of the minimization problem described in Eq. (3) provides the tomographic reconstruction of the T and X distributions.

3. Experimental arrangement

A measurement campaign was conducted to apply the HT technique to the exhaust stream of the augmentor-equipped J85-GE-5 gas turbine engine located at the University of Tennessee Space Institute (UTSI). This engine is operated by personnel affiliated with the Air Force Arnold Engineering and Development Center (AEDC) and has been developed and used as a test bed for evaluation of advanced diagnostic techniques [23].

An overview of the experimental arrangement is shown in Fig. 2. The UTSI test facility consists of a high-bay room which contains the J85 engine and a control room located in an adjacent building. The HT sensor was installed on a tomography frame, which held the sensor at the exhaust plane of the engine as shown. The HT sensor utilized 32 laser beams, generated by a laser system consisting of three independent Fourier-domain mode-locked (FDML) lasers [24]. These lasers were placed in the control room, and their operation was synchronized and controlled by a master clock and three function generators (FG). The laser beams generated were then delivered to the measurement location by single-mode fibers (SMF), with length of ~60 m. A 4×32 multiplexer was used to combine and distribute the laser beams over the required 32 channels needed for the experiment. The multiplexer was placed near the engine to minimize the length needed for the test-section delivery fibers. A total of 30 laser beams coming out of the multiplexer were used for the actual measurements: 15 of them installed to probe the measurement plane horizontally and 15 vertically (more details shown in Fig. 3), forming a square mesh of 225 grid points over which the tomography reconstruction was performed according to the method described in Section 2. The remaining two laser beams coming out of the multiplexer were used for laser referencing: one of them was sent to a photodiode to record the laser intensity and the other directed to a Mach-Zehnder interferometer to monitor the wavelength scan. The data-acquisition system was placed near the engine (~15 m away from the engine) to minimize the required length of

coaxial cable. Cost was the primary motivation for minimizing the length of the fiber and cable.
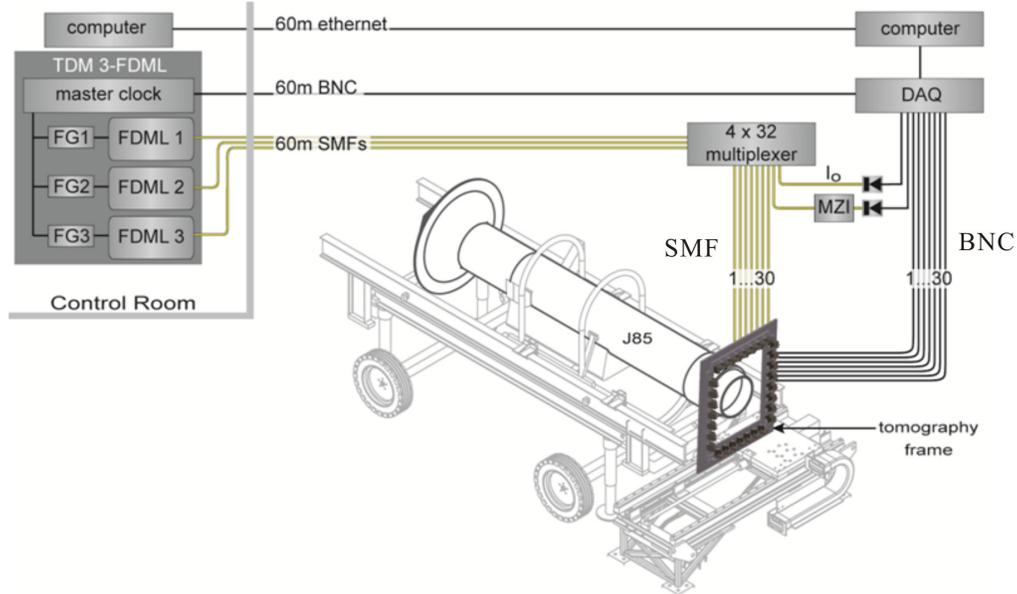

Fig. 2. Overview of the experimental setup with a 30-beam HT sensor applied at the exhaust stream of a J85 engine. The laser system (labeled as TDM 3-FDML) was operated from the facility control room and 60-m-long optical fibers were used to transmit the laser signals to the engine location. A 4 × 32 multiplexer located near the engine was used to combine and split the three laser signals into 32 independent outputs. A customer-built tomography frame was mounted at the measurement location (the exit plane of the exhaust nozzle), holding the probe laser beams in position to create the 15 × 15 grid pattern for the tomographic reconstruction.

Figure 3 provides a more detailed illustration of the HT sensor and its installation. The 30 probe beams were installed on a customer-built aluminum frame, which was designed both to hold the probe beams at the measurement plane and also to protect the electro-optic components from the high-temperature and -velocity combustion flow. Panel (a) shows the configuration of the probe beams: 15 installed horizontally and 15 vertically, with a spacing of 38.3 mm (1.5 inches) between probe beams. Panel (b) shows a photograph of the frame and the optical components (with a measured temperature distribution superimposed in the middle). The frame consisted of a square base plate with an opening sized to match the diameter of the exit shroud of the J85 engine 45.72 cm (18 inches). On each of the four sides of the frame, two sets of rails were fabricated and used to mount the fiber collimators and detectors. Each of the 30 probe beams consisted of a laser delivery fiber (Corning SMF-28), a collimating lens, free-space path across the test section, a collection lens, and a photodetector. The collimating lens used was a 1.25-mm-diameter plano/convex fused silica rod-shape lens with a designed working distance of 92 mm at a wavelength of 1310 nm. The plano side of the collimating lens was fused directly to the end of the SMF, and the entire collimating assembly was held in a kinematic stage for beam-alignment purposes. A plano-convex lens with a diameter of 25.4 mm was used to collect and focus light onto the photodetector (Thorlabs PDA10CF, with an active area with 0.5-mm diameter). Panel (c) depicts the location of the measurements plane in the exhaust and a sample measurement of the 2D distribution of the temperature measured at this location. The analog voltage signal from the detector was transferred via coaxial cable to a National Instruments PXI-5105 data-acquisition board for digitization and subsequent data storage on a personal computer.
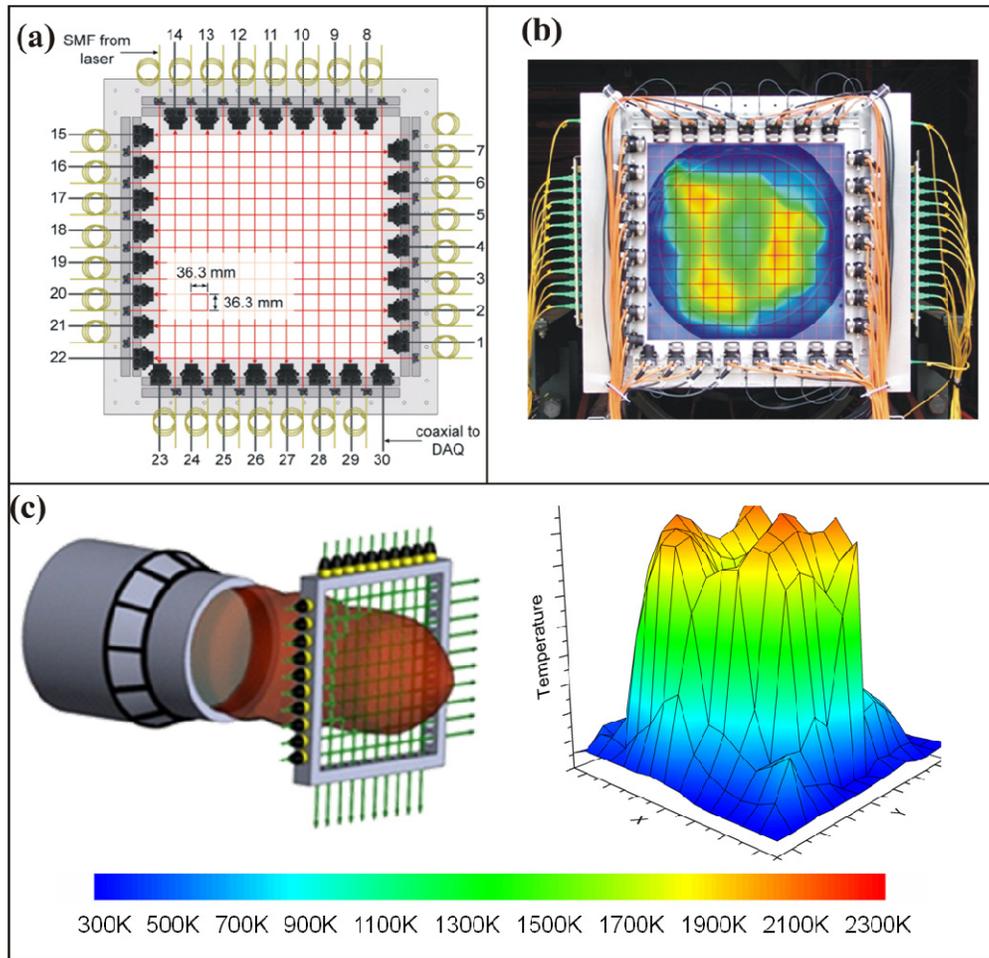
Fig. 3. Schematic representation of the optical test section hardware. A 15 x 15 crossing beam grid pattern with a 36.3-mm beam spacing was used for the tomographic reconstruction. Light from the laser was delivered to the test section via single-mode fibers (SMF) and was collimated and transmitted across the engine exhaust flow. 1-in collection lenses were used on the receiving side and focused the laser light onto photodiodes. Panel (a): configuration of the probe beams. Panel (b): a photograph of the frame and the optical components overlaid by a sample reconstruction to illustrate the location of the flowfield. Panel(c): schematic of the location of the measurements plane in the exhaust and a sample measurement of the 2D distribution of the temperature measured at this location.

4. Hyperspectral laser source

A key component in the HT sensor is the hyperspectral laser source, which enabled the measurement of a large number of absorption transitions across a wide spectral range at high repetition rate. The laser source chosen for this work was a time-division-multiplexed (TDM) combination of three FDML lasers, hereafter referred to as the TDM 3-FDML system. This system operates near 1350 nm to monitor H_2O vapor absorption features. TDM has been used in H_2O vapor absorption spectroscopy for years [25]. Recently developed TDM lasers for H_2O absorption spectroscopy offer enhanced capabilities. For example, a recent TDM laser concept enabled rapid monitoring of numerous (10s to 100s) discrete spectral channels [26] and was successfully used to monitor gas temperature and H_2O and CH_4 concentrations in a high-pressure gas turbine combustor rig operated at the Air Force Research Laboratory (AFRL) [27].

Structurally, the three FDML lasers used in this work were virtually identical. Each was configured to output a high-repetition-rate (~50-kHz) wavelength sweep over a unique ~10 cm^{-1} spectral range. In our earlier work where one FDML laser was used for H_2O absorption spectroscopy for the first time [24], a single FDML was configured to sweep a much broader range (~150 cm^{-1}). By multiplexing 3 FDMLs in this work, we focused on three spectral regions of the H_2O spectrum with the highest temperature sensitivity to reduce the data-acquisition load relative to our initial work. Because the center wavelength and sweep range of each of the 3 FDMLs can be independently adjusted [28], the TDM 3-FDML source can be optimized for each test article of interest. For example, when the gas pressure within the test environment is high (e.g., 30 bar) the sweep range of each FDML is generally increased to allow more complete monitoring of the shapes of spectral features. When the gas temperatures within the test environment are confined to some limited range, the center wavelengths of the 3 FDMLs can be chosen to offer maximum temperature sensitivity within that range. In this work, the test gas was near atmospheric pressure, so we chose relatively narrow wavelength sweeps (~10 cm^{-1} each); the temperatures were expected to span 300–2300 K, so we chose features that maximized the overall temperature sensitivity over this wide range of temperatures, following an approach similar to that described in reference [29].

Because each FDML sweeps a ~10 cm^{-1} range, absorption baselines can be accurately determined along with *in situ* feature lineshapes. The latter capability reduces the need to rely on auxiliary measurements of gas pressure and offers the potential for gas pressure measurements in addition to the usual targets (gas temperature and H_2O mole fraction).

The TDM 3-FDML laser was designed for multi-beam tomographic measurements based on H_2O absorption spectroscopy. The three FDML cavity lengths were matched to within 3 cm (cavity lengths: ~3020 m) in order to operate the fiber Fabry-Perot tunable filters (FFP-TFs) at the same frequency: 50.24337 kHz (the overall repetition rate of the TDM 3-FMDL system). Because of the high number of output beams, each of the three FDML output signals was amplified with an external-cavity semiconductor optical amplifier (SOA) to compensate for the multiplexing loss (−15 dB for 32 fiber-coupled outputs, neglecting excess loss). Pulsing each of these SOAs at ~33% duty cycle facilitated time-division multiplexing of the 3 FDMLs and allowed selection of the middle of the blue-to-red sweep of each laser. The injection current to each external-cavity SOA was provided by an off-the-shelf diode laser controller (Wavelength Electronics, LDTC 2/2 E, 2-MHz modulation bandwidth). The gate signals to the diode-laser controllers were provided by a pulse generator (Berkeley Nucleonics Corporation, BNC555) that was locked with the three FFP-TF drive signal generators (FG, Agilent 33220A) to a synthesized clock generator (Stanford Research Systems, SRS CG635). The entire laser system was housed in a transportable 19-inch rack enclosure.

5. Results and discussions

Measurements were performed on the J85 engine under different conditions including ground-idle, full-military, and full-afterburner operation. Figure 4 shows a sample set of the spectra measured by the TDM 3-FDML laser during one single scan under full-afterburner operation. Each panel shows the spectra measured by one FDML laser during that scan at two beam locations (illustrated by the red and blue arrows in the right panel). These two beams locations were chosen to represent a "hot beam" and a "cold beam, beams 4 and 22 illustrated by the red and blue arrow in the right panel, respectively. The hot beam (beam 4) passes through the center of the engine exhaust, along which the temperature distribution varies significantly more than that along the cold beam, which passes through the edge of the exhaust stream. As a result of such different temperature distributions, the spectra measured at the hot and cold beam locations also differ as shown in Fig. 4. Such difference forms the basis for the tomographic reconstruction discussed in Section 2.

A smaller set of absorption transitions can be selected out of those monitored by the three FDML lasers, as shown in Fig. 4, for two considerations. First, not all the transitions shown in

Fig. 4 are equally valuable for the tomographic reconstruction [30]. Second, consideration of computational cost also motivates the use of a smaller set of transitions [21], because the computational cost is approximately proportional to the number of transitions used in the tomographic reconstruction. In this work, we selected a total of 12 transitions out of those shown in Fig. 4 according to the method described in [30] for the tomographic reconstruction. Absorption measured at these 12 selected wavelengths was then used as inputs to Eq. (3) to perform the tomographic inversion.
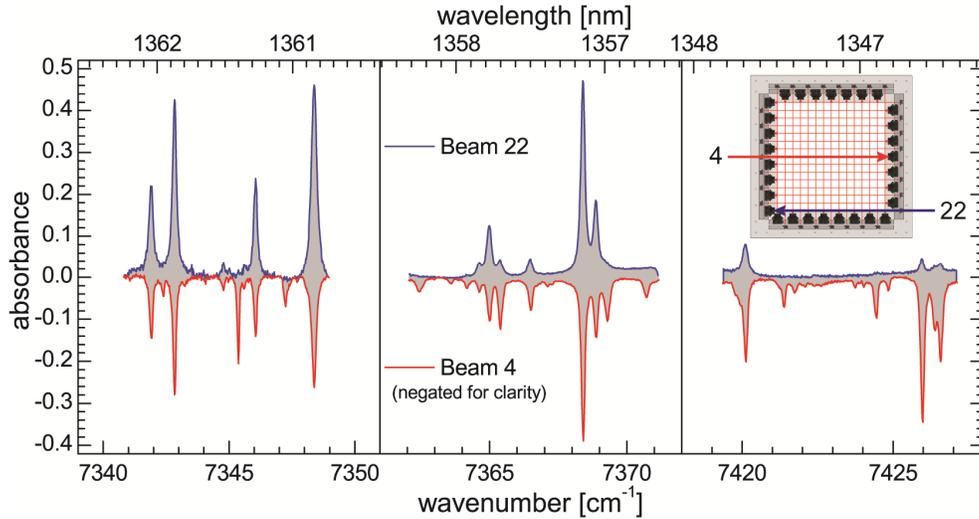
Fig. 4. Absorption spectra measured during a single scan of the TDM 3-FDML laser operating at 50.24337 kHz (~20 microseconds). Each panel shows the spectra measured by one of the three FDML lasers.

Figure 5 shows a set of sample results of the temperature and H_2O mole-fraction distributions measured under representative conditions in the J85 engine. Under all conditions, the measurements were taken at 50 kHz; and the tomographic algorithm was applied to process the measurements frame by frame to obtain distributions of temperature and H_2O mole fraction. Under each representative operation condition (ground idle, full military, and full afterburner), a total of 100 frames were processed to make the video shown in this paper, corresponding to 2 ms of measurement duration. Each panel of Fig. 5 shows one frame, arbitrarily chosen out of 100 frames of measurements. Note that panel (a) (Media 1), (b) (Media 2), and (c) (Media 3) show temperature results with the color scale shown next to panel (b) (Media 2); and panel (d) shows H_2O mole-fraction results with the color scale shown next to it.
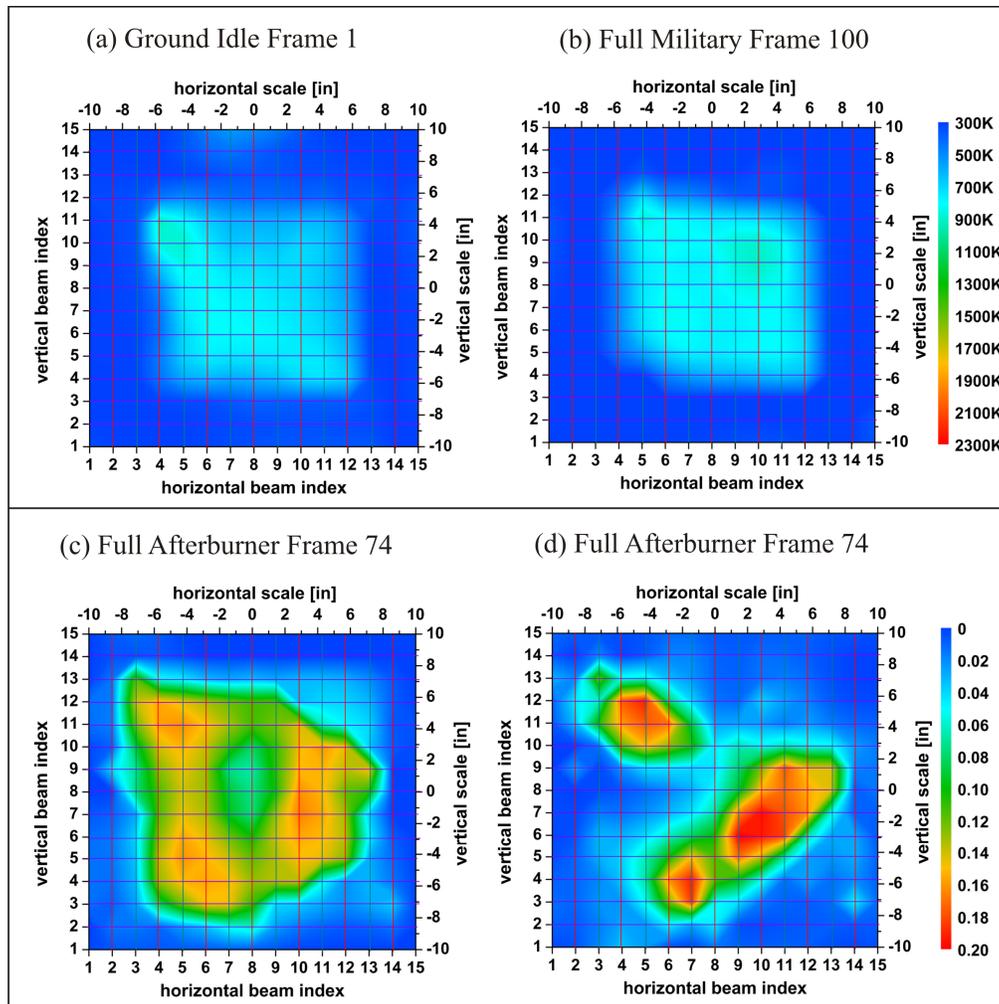
Fig. 5. A set of sample results obtained in the J85 engine. Each panel shows one frame, arbitrary chosen out of 100 frames of measurements, corresponding to 2 ms of measurement duration. Panel (a): frame 1 of temperature distribution under ground-idle operation (Media 1). Panel (b): frame 100 of temperature distribution under full military operation (Media 2). Panel (c): frame 74 of temperature distribution full-afterburner operation (Media 3). Panel (d): frame 74 of H_2O mole-fraction distribution under full-afterburner operation.

The reconstructions shown in Fig. 5 were obtained based on a square domain of measurement, even though the flowfield was circular. This work defined a square domain of measurement by the tips of the collimating lenses and the tips of the collection lenses, as shown in Panels (a) and (b) of Fig. 3. This square region was then discretized into grids of size 36.3×36.3 mm as shown in Panel (a) of Fig. 3 for the tomographic reconstruction.

As noted in the introduction, several key advantages of the HT technique were demonstrated in these applications in comparison to other well-established techniques such as PLIF and Rayleigh scattering. First, the HT technique extensively utilizes fiber technologies, which greatly facilitate its application in practical combustion devices and field measurements as depicted in Fig. 2 and Fig. 3. Second, the HT technique enables a temporal resolution that is comparable to planar techniques using state-of-the-art laser and camera techniques. Third, the HT technique, though unable to compete with planar techniques in terms of the spatial resolution, provides the ability to monitor a relatively large FOV. Based on these previous applications, with additional capital investment, it is relatively

straightforward to add additional laser beams to enhance the spatial resolution. Because of these advantages, we expect the HT technique to play unique roles in the study of high-speed reactive flow, in the diagnosis of practical propulsion devices, and eventually in the active control and monitoring of such devices.

6. Summary

This paper reports a new laser diagnostic that can measure 2D distribution of temperature and H_2O concentration simultaneously with a temporal resolution of 50 kHz at 225 spatial grid points. To our knowledge, it is the first time that such measurement capabilities have been reported. The diagnostic technique leverages recent developments in hyperspectral laser sources and fiber technologies, so that 1) a large number of absorption transitions can be measured over a relatively wide spectral range with a rapid repetition rate, and 2) the probe laser can be split and delivered to perform measurements at multiple spatial locations. A mathematical formulation and a corresponding algorithm have been developed to exploit the multi-spectral and multi-spatial information, yielding 2D tomography imaging of the temperature and H_2O concentration distribution.

The HT technique has been demonstrated in the exhaust plane of a practical aero-propulsion engine (General Electric J85). Simultaneous imaging measurement of the distribution of temperature and H_2O concentration were obtained at a rate of 50 kHz under different engine operation conditions. The application in a practical aero-propulsion engine demonstrated several unique advantages of the HT technique, including its robustness and ease of implementation in practical systems, and its ability to perform measurements across a relatively large FOV. These advantages are expected to contribute to some critical issues in aero-propulsion systems, such as combustion instability and thermal-acoustic coupling.

Acknowledgments